Tuovinen, Toni; Hinkkanen, Marko; Harnefors, Lennart; Luomi, Jorma

# Comparison of a reduced-order observer and a full-order observer for sensorless synchronous motor drives

*Document Version*
Peer-reviewed accepted author manuscript, also known as Final accepted manuscript or Post-print

# Comparison of a Reduced-Order Observer and a Full-Order Observer for Sensorless Synchronous Motor Drives

Toni Tuovinen, Marko Hinkkanen, *Member, IEEE*, Lennart Harnefors, *Senior Member, IEEE*, and Jorma Luomi, *Member, IEEE*

*Abstract*—Two back-electromotive-force (EMF)-based position observers are compared for motion-sensorless synchronous motor drives: the reduced-order observer and the adaptive full-order observer. A stabilizing gain is proposed for the adaptive full-order observer, which guarantees the local stability of the closed-loop system, if the motor parameters are known. Equations for the steady-state position error and for the linearized estimation-error dynamics under erroneous parameters are derived, and the robustness of the two observers against parameter errors is analyzed and compared. The observers are experimentally evaluated using a 6.7-kW synchronous reluctance motor drive in low-speed operation and under parameter errors. The gain selection of the reduced-order observer is easier, but the adaptive full-order observer can be made more robust against parameter variations and noise.

*Index Terms*—Observer, parameter uncertainties, permanent-magnet synchronous motor, sensorless, stability conditions, synchronous reluctance motor.

## I. INTRODUCTION

Because of lower losses, the permanent-magnet synchronous motor (PMSM) has during the last decades emerged as an attractive alternative to the induction motor in variable-speed drives. Recent design improvements have also allowed the synchronous reluctance motor (SyRM) to become a contender [1], [2], [3]. A magnetizing current component is necessary in the stator winding of the SyRM, but field weakening is straightforward as compared to the PMSM. The recent price increase of rare-earth metals has also made the SyRM more favorable in relation to the PMSM.

For both motor types and for well-known reasons, position-sensorless operation is desirable. As the SyRM is inherently salient, signal-injection methods [4], [2], [5], [6] are readily applicable for rotor-position estimation. A position estimate of near zero error at all speeds, including standstill, can be obtained. (There will, however, be an uncertainty of 180 degrees, as there is no rotor excitation or permanent magnets.)

Although some authors favor the usage of signal-injection methods at all speeds [7], it is often desirable to avoid additional noise and losses by using a back-EMF-based position

estimation method, combined with a signal-injection method applied only at the lowest speeds [8], [9], [10]. Since the SyRM can be seen as a special case of the salient PMSM, back-EMF-based methods suitable for salient PMSMs, for example the observers proposed in [8], [11], [12], can be used for SyRMs with slight modifications.

In this paper, two back-EMF-based observers will be compared: a reduced-order observer [8], [12] and an adaptive full-order observer [11].[1] A minimum requirement for any observer is that the estimation-error dynamics of the closed-loop system are locally stable at every operating point (except at zero speed) in ideal conditions. In order to satisfy this requirement and to simplify the tuning procedure, a general stabilizing gain was derived for the reduced-order observer in [12]. A general stabilizing gain was proposed for a full-order observer variant in [13], but the dynamics of the d-axis current were omitted in the case of the salient PMSM.

The observer design affects also the sensitivity to motor model parameter errors and noise. The actual parameters are rarely known accurately, and in practice, they are not constant. The inductances vary due to the magnetic saturation, and the stator resistance and the permanent-magnet (PM) flux depend on the temperature. The noise in the sensorless drive system typically originates from the measurements and, on the other hand, from nonidealities of the motor. For example, unmodelled spatial harmonics (in the stator inductance and the PM flux) and saturation-induced harmonics may cause disturbances in the rotor-position estimate [14], [15]. The estimation errors caused by the parameter errors and noise can be reduced by means of the observer design.

After a review of the motor model in Section II, the main contributions of the paper are presented:

1) A stabilizing gain for the full-order observer, applicable also to the salient PMSM, is proposed in Section III.
2) Equations for the steady-state position error and for the linearized estimation-error dynamics under erroneous parameters are derived in Section IV, and the robustness of the reduced-order observer and the full-order observer against parameter errors is analyzed and compared.

The experimental setup is described in Section V, and the sensitivity of the two observers to the parameter errors and

[1]The reduced-order observer and the full-order observer can easily be augmented with a signal-injection method at lowest speeds in a fashion similar to [8] and [11], respectively. For brevity, these augmentations will not be addressed explicitly in this paper.

noise is experimentally compared using a 6.7-kW SyRM drive in Section VI.

## II. MOTOR MODEL

Real space vectors will be used. For example, the stator-current vector is $\boldsymbol{i}_s = [i_d, i_q]^T$, where $i_d$ and $i_q$ are the components of the vector and the matrix transpose is marked with the superscript T. The orthogonal rotation matrix is defined as

$$\mathbf{J} = \begin{bmatrix} 0 & -1 \\ 1 & 0 \end{bmatrix}.$$

The electrical angular position of the direct axis is denoted by $\vartheta_m$. The direct axis is defined as the direction of the PM flux for PMSMs, and as the direction of the maximum inductance for SyRMs. The position depends on the electrical angular rotor speed $\omega_m$ according to

$$\frac{d\vartheta_m}{dt} = \omega_m. \tag{1a}$$

To simplify the analysis in the following sections, the machine model will be expressed in the *estimated* rotor coordinates, whose d-axis is aligned at $\hat{\vartheta}_m$ with respect to the stator coordinates. The stator inductance matrix and the PM-flux vector, respectively, are

$$\boldsymbol{L} = e^{-\tilde{\vartheta}_m \mathbf{J}} \begin{bmatrix} L_d & 0 \\ 0 & L_q \end{bmatrix} e^{\tilde{\vartheta}_m \mathbf{J}}, \quad \boldsymbol{\psi}_{pm} = e^{-\tilde{\vartheta}_m \mathbf{J}} \begin{bmatrix} \psi_{pm} \\ 0 \end{bmatrix} \tag{1b}$$

where $\tilde{\vartheta}_m = \hat{\vartheta}_m - \vartheta_m$ is the estimation error in the rotor position, $L_d$ the direct-axis inductance, $L_q$ the quadrature-axis inductance, and $\psi_{pm}$ the PM flux. The stator-voltage equation is

$$\frac{d\boldsymbol{\psi}_s}{dt} = \boldsymbol{u}_s - R_s \boldsymbol{i}_s - \hat{\omega}_m \mathbf{J} \boldsymbol{\psi}_s \tag{1c}$$

where $\boldsymbol{\psi}_s$ is the stator-flux vector, $\boldsymbol{u}_s$ the stator-voltage vector, $R_s$ the stator resistance, and $\hat{\omega}_m = d\hat{\vartheta}_m/dt$ is the angular speed of the coordinate system. The stator current is a non-linear function

$$\boldsymbol{i}_s = \boldsymbol{L}^{-1} \left( \boldsymbol{\psi}_s - \boldsymbol{\psi}_{pm} \right) \tag{1d}$$

of the stator-flux vector and the position error $\tilde{\vartheta}_m$. There are two special cases of the synchronous-motor model: nonsalient PMSMs ($L_d = L_q$) and SyRMs ($\psi_{pm} = 0$).

## III. ROTOR-POSITION OBSERVERS

### A. Reduced-Order Observer

The reduced-order observer proposed in [12] is considered. It is based on estimating the rotor position and the d component $\hat{\psi}_d$ of the stator flux in the estimated rotor coordinates. The componentwise presentation of the observer is

$$\frac{d\hat{\psi}_d}{dt} = u_d - \hat{R}_s i_d + \hat{\omega}_m \hat{L}_q i_q + k_1(\hat{\psi}_d - \hat{L}_d i_d - \hat{\psi}_{pm}) \tag{2a}$$

$$\frac{d\hat{\vartheta}_m}{dt} = \frac{u_q - \hat{R}_s i_q - \hat{L}_q \frac{di_q}{dt} + k_2(\hat{\psi}_d - \hat{L}_d i_d - \hat{\psi}_{pm})}{\hat{\psi}_d} \tag{2b}$$

where $\hat{L}_d$ and $\hat{L}_q$ are the model d- and q-axis inductances, respectively, $\hat{R}_s$ is the model stator resistance, and $\hat{\psi}_{pm}$ is

the model PM-flux magnitude. The observer is of the second order, and there are only two gains, $k_1$ and $k_2$.

With accurate model parameters, the closed-loop system consisting of (1) and (2) is locally stable in every operating point if the gains are given by [12]

$$k_1 = -\frac{b + \hat{\beta}(c/\hat{\omega}_m - \hat{\omega}_m)}{\hat{\beta}^2 + 1}, \quad k_2 = \frac{\hat{\beta}b - c/\hat{\omega}_m + \hat{\omega}_m}{\hat{\beta}^2 + 1} \tag{3}$$

where the design parameters $b > 0$ and $c > 0$ may depend on the operating point and

$$\hat{\beta} = \frac{(\hat{L}_d - \hat{L}_q)i_q}{\hat{\psi}_{pm} + (\hat{L}_d - \hat{L}_q)i_d}. \tag{4}$$

The parameters $b$ and $c$ are actually the coefficients of the characteristic polynomial, $s^2 + bs + c$, of the linearized system consisting of (1) and (2). As a special case, the relation between the two design parameters for SyRMs can be chosen as

$$c = \sqrt{3}b|\hat{\omega}_m| + \hat{\omega}_m^2 \tag{5}$$

which guarantees maximum robustness against parameter errors in low-speed operation [15]. The observer can be easily augmented with a stator-resistance adaptation law, cf. [12].

### B. Adaptive Full-Order Observer

*1) Observer Structure:* In the adaptive full-order observer [16], [11], both stator-flux vector components are estimated. The matrix presentation of the observer in the estimated rotor coordinates is

$$\frac{d\hat{\boldsymbol{\psi}}_s}{dt} = \boldsymbol{u}_s - \hat{R}_s \hat{\boldsymbol{i}}_s - \hat{\omega}_m \mathbf{J} \hat{\boldsymbol{\psi}}_s + \boldsymbol{K} \tilde{\boldsymbol{i}}_s \tag{6a}$$

$$\hat{\boldsymbol{i}}_s = \hat{\boldsymbol{L}}^{-1} \left( \hat{\boldsymbol{\psi}}_s - \hat{\boldsymbol{\psi}}_{pm} \right) \tag{6b}$$

where $\hat{\boldsymbol{i}}_s$ is the estimated stator-current vector, $\tilde{\boldsymbol{i}}_s = \hat{\boldsymbol{i}}_s - \boldsymbol{i}_s$ is the estimation error of the stator current, and $\boldsymbol{K}$ is a $2 \times 2$ observer gain matrix. The model inductance matrix and the model PM-flux vector are

$$\hat{\boldsymbol{L}} = \begin{bmatrix} \hat{L}_d & 0 \\ 0 & \hat{L}_q \end{bmatrix}, \quad \hat{\boldsymbol{\psi}}_{pm} = \begin{bmatrix} \hat{\psi}_{pm} \\ 0 \end{bmatrix} \tag{6c}$$

respectively. The rotor speed is estimated with the PI mechanism

$$\hat{\omega}_m = \boldsymbol{k}_p \tilde{\boldsymbol{i}}_s + \boldsymbol{k}_i \int \tilde{\boldsymbol{i}}_s dt. \tag{7a}$$

where the gain vectors $\boldsymbol{k}_p$ and $\boldsymbol{k}_i$ are chosen to utilize the estimation error only in the q-axis direction,

$$\boldsymbol{k}_p = [0, k_p], \quad \boldsymbol{k}_i = [0, k_i]. \tag{7b}$$

It can be seen that the observer is of the fourth order. The characteristics of the closed-loop system depend on the choice of the gains $\boldsymbol{K}$, $k_p$, and $k_i$.

*2) Proposed Stabilizing Gain:* The proposed stabilizing gain matrix is

$$\boldsymbol{K} = \begin{bmatrix} \hat{R}_{\mathrm{s}} + \hat{L}_{\mathrm{d}}k_1 & -\hat{L}_{\mathrm{q}}\hat{\beta}k_1 \\ \hat{L}_{\mathrm{d}}k_2 & \hat{R}_{\mathrm{s}} - \hat{L}_{\mathrm{q}}\hat{\beta}k_2 \end{bmatrix} \tag{8}$$

where $k_1$ and $k_2$ are given by (3). With this gain selection and accurate model parameters, the characteristic polynomial of the closed-loop system consisting of (1) and (6)–(8) can, after linearization, be split into a product of two second-order polynomials,

$$(s^2 + bs + c)\left(s^2 + k_{\mathrm{p}}\frac{\hat{\beta}_{\mathrm{den}}}{\hat{L}_{\mathrm{q}}}s + k_{\mathrm{i}}\frac{\hat{\beta}_{\mathrm{den}}}{\hat{L}_{\mathrm{q}}}\right) \tag{9}$$

where

$$\hat{\beta}_{\mathrm{den}} = \hat{\psi}_{\mathrm{pm}} + (\hat{L}_{\mathrm{d}} - \hat{L}_{\mathrm{q}})i_{\mathrm{d}} \tag{10}$$

is the denominator of (4). For convenience, the gains $k_{\mathrm{p}}$ and $k_{\mathrm{i}}$ are selected according to

$$k_{\mathrm{p}} = \frac{\hat{L}_{\mathrm{q}}d}{\hat{\beta}_{\mathrm{den}}}, \quad k_{\mathrm{i}} = \frac{\hat{L}_{\mathrm{q}}e}{\hat{\beta}_{\mathrm{den}}} \tag{11}$$

which simplifies the characteristic polynomial to

$$(s^2 + bs + c)(s^2 + ds + e). \tag{12}$$

Coefficients $b$, $c$, $d$, and $e$ are design parameters, which may depend on the operating point. The local stability of the closed-loop estimation error dynamics are guaranteed, if all four design parameters are positive.

The proposed observer design is a subset of all stable designs, since the gain matrix (8) has only two free parameters instead of four. With the proposed design, however, the tuning procedure based on (12) is considerably simpler than that of a more general fourth-order polynomial. As compared to [13], the analysis here is also valid when $\mathrm{d}i_{\mathrm{d}}/\mathrm{d}t \neq 0$. The only assumptions are that the parameters are constant, and the model parameters are accurate.

In order to reduce the number of design parameters, $d$ and $e$ can be chosen as [17]

$$d = 2\rho, \quad e = \rho^2 \tag{13}$$

yielding double pole located at $s = -\rho$. The remaining three design parameters are $b$, $c$, and $\rho$, which should be positive.

## IV. Stability With Uncertain Parameters

The stability of the estimation-error dynamics with accurate model parameters is necessary but not a sufficient design goal, since the system should be robust against parameter errors. With erroneous model parameters, the stability is not guaranteed for all positive values of the design parameters. In the following, it is studied how the design parameters should be chosen in order to reduce sensitivity to parameter errors. For both observers, the local stability of the estimation-error dynamics are analyzed in the vicinity of a steady-state position error $\tilde{\vartheta}_{\mathrm{m0}}$, which is nonzero due to parameter errors. Equations are given in the general from, while the data of a 6.7-kW SyRM are used in the examples.

### A. Steady-State Estimation Error

The speed-adaptation law (7) drives $\tilde{i}_{\mathrm{q}}$ to zero in steady state, while the adaptation gains do not affect the steady-state position error. It can be shown that the equation for the steady-state position error $\tilde{\vartheta}_{\mathrm{m0}}$ for both the reduced-order observer and the adaptive full-order observer is[2]

$$A\cos(2\tilde{\vartheta}_{\mathrm{m0}}) + B\sin(2\tilde{\vartheta}_{\mathrm{m0}}) + C\cos\tilde{\vartheta}_{\mathrm{m0}} \\ + D\sin\tilde{\vartheta}_{\mathrm{m0}} + E = 0 \tag{14a}$$

where

$$A = (L_{\mathrm{d}} - L_{\mathrm{q}})[i_{\mathrm{q}}(k_2 - \omega_{\mathrm{m}}) - i_{\mathrm{d}}k_1] \tag{14b}$$

$$B = (L_{\mathrm{d}} - L_{\mathrm{q}})[i_{\mathrm{d}}(k_2 - \omega_{\mathrm{m}}) + i_{\mathrm{q}}k_1] \tag{14c}$$

$$C = -2k_1\psi_{\mathrm{pm}} \tag{14d}$$

$$D = 2\psi_{\mathrm{pm}}(k_2 - \omega_{\mathrm{m}}) \tag{14e}$$

$$E = -C - A + 2[i_{\mathrm{q}}k_1 - i_{\mathrm{d}}(k_2 - \omega_{\mathrm{m}})]\tilde{R}_{\mathrm{s}}/\omega_{\mathrm{m}} \\ + 2k_1(\tilde{\psi}_{\mathrm{pm}} + i_{\mathrm{d}}\tilde{L}_{\mathrm{d}}) + 2i_{\mathrm{q}}(k_2 - \omega_{\mathrm{m}})\tilde{L}_{\mathrm{q}}. \tag{14f}$$

The estimation error of the PM flux is defined as $\tilde{\psi}_{\mathrm{pm}} = \hat{\psi}_{\mathrm{pm}} - \psi_{\mathrm{pm}}$ and other estimation errors are defined similarly.

It can be seen from the coefficients that the error in the q-axis inductance does not affect the steady-state position error in no-load condition. The ratio $\tilde{R}_{\mathrm{s}}/\omega_{\mathrm{m}}$ is the most crucial factor in low-speed operation. In order to reduce the sensitivity of the position error to parameter errors $\tilde{\psi}_{\mathrm{pm}}$ and $\tilde{L}_{\mathrm{d}}$, the absolute value of the gain $k_1$ should be small. Similarly, to reduce the sensitivity to the parameter error $\tilde{L}_{\mathrm{q}}$, the absolute value of $k_2 - \omega_{\mathrm{m}}$ should be small.

In order to achieve good transient response, at least one of the poles of the closed-loop system must be fast. For the reduced-order observer, this is obtained by choosing a large value for the coefficient $b$, which results in large values for $k_1$ and $k_2$. For the adaptive full-order observer, the fast dynamics can be provided by the speed-adaptation loop, while the coefficients $b$ and $c$ can be kept small. This results in decreased parameter sensitivity, as can be seen from (14).

In the general case, the steady-state position error should be solved numerically, but the solution can be easily written for nonsalient PMSMs or SyRMs. For SyRMs, the solution for the steady-state position error is

$$\tilde{\vartheta}_{\mathrm{m0}} = -\frac{\sin^{-1}\left(\frac{E}{F}\right) + \phi}{2} \tag{15a}$$

where

$$\phi = \tan^{-1}\left(\frac{A}{B}\right), \quad F = \frac{B}{\cos\phi}. \tag{15b}$$

The general solutions for the steady-state flux errors $\tilde{\psi}_{\mathrm{d0}}$ and $\tilde{\psi}_{\mathrm{q0}}$ for both the reduced-order observer and the adaptive

---

[2]With a general choice of the gain vectors $\boldsymbol{k}_{\mathrm{p}}$ and $\boldsymbol{k}_{\mathrm{i}}$, the coefficients in (14) would be functions of the components of $\boldsymbol{k}_{\mathrm{p}}$ and $\boldsymbol{k}_{\mathrm{i}}$ in the case of the adaptive full-order observer. This is avoided by using a projection (7b) only in the q-axis direction.

$$\frac{\mathrm{d}}{\mathrm{d}t}\begin{bmatrix}\tilde{\psi}_{\mathrm{d}}\\\tilde{\psi}_{\mathrm{q}}\\\tilde{\vartheta}_{\mathrm{m}}\\\tilde{\omega}_{\mathrm{m}}\end{bmatrix}=\begin{bmatrix}k_1 & -k_1\hat{\beta}+\omega_{\mathrm{m}} & k_1(\hat{\beta}\beta_{\mathrm{den}}-\beta_{\mathrm{num}}) & \tilde{\psi}_{\mathrm{q}0}\\k_2-\omega_{\mathrm{m}} & -k_2\hat{\beta} & k_2(\hat{\beta}\beta_{\mathrm{den}}-\beta_{\mathrm{num}}) & -\tilde{\psi}_{\mathrm{d}0}\\0 & 0 & 0 & 1\\\dfrac{d(k_2-\omega_{\mathrm{m}})}{\hat{\beta}_{\mathrm{den}}} & \dfrac{e-dk_2\hat{\beta}}{\hat{\beta}_{\mathrm{den}}} & \dfrac{d(\hat{\beta}\beta_{\mathrm{den}}-\beta_{\mathrm{num}})k_2-e\beta_{\mathrm{den}}}{\hat{\beta}_{\mathrm{den}}} & -d\dfrac{\beta_{\mathrm{den}}+\tilde{\psi}_{\mathrm{d}0}}{\hat{\beta}_{\mathrm{den}}}\end{bmatrix}\begin{bmatrix}\tilde{\psi}_{\mathrm{d}}\\\tilde{\psi}_{\mathrm{q}}\\\tilde{\vartheta}_{\mathrm{m}}\\\tilde{\omega}_{\mathrm{m}}\end{bmatrix}\tag{19}$$

full-order observer are

$$\tilde{\psi}_{\mathrm{d}0}=\frac{2\tilde{R}_{\mathrm{s}}i_{\mathrm{q}}+k_2(2\hat{\beta}_{\mathrm{den}}-\beta_{\mathrm{den}})}{2(k_2-\omega_{\mathrm{m}})}$$
$$-\frac{k_2[\psi_{\mathrm{pm}}\cos\tilde{\vartheta}_{\mathrm{m}0}+(L_{\mathrm{d}}-L_{\mathrm{q}}+2\tilde{L}_{\mathrm{q}})i_{\mathrm{d}}]}{2(k_2-\omega_{\mathrm{m}})}\tag{16a}$$

$$\tilde{\psi}_{\mathrm{q}0}=\frac{\psi_{\mathrm{pm}}\sin\tilde{\vartheta}_{\mathrm{m}0}-(L_{\mathrm{d}}-L_{\mathrm{q}}-2\tilde{L}_{\mathrm{q}})i_{\mathrm{q}}+\beta_{\mathrm{num}}}{2}\tag{16b}$$

where

$$\beta_{\mathrm{num}}=\psi_{\mathrm{pm}}\sin\tilde{\vartheta}_{\mathrm{m}0}+(L_{\mathrm{d}}-L_{\mathrm{q}})i_{\mathrm{q}}\cos(2\tilde{\vartheta}_{\mathrm{m}0})$$
$$+(L_{\mathrm{d}}-L_{\mathrm{q}})i_{\mathrm{d}}\sin(2\tilde{\vartheta}_{\mathrm{m}0})\tag{17a}$$

$$\beta_{\mathrm{den}}=\psi_{\mathrm{pm}}\cos\tilde{\vartheta}_{\mathrm{m}0}+(L_{\mathrm{d}}-L_{\mathrm{q}})i_{\mathrm{d}}\cos(2\tilde{\vartheta}_{\mathrm{m}0})$$
$$-(L_{\mathrm{d}}-L_{\mathrm{q}})i_{\mathrm{q}}\sin(2\tilde{\vartheta}_{\mathrm{m}0}).\tag{17b}$$

### B. Reduced-Order Observer

The effects of the design parameters on the robustness of the reduced-order observer have been analyzed in [12] and [15]. For comparison purposes, the analysis method and some results are briefly reviewed here.

The estimation error dynamics of the reduced-order observer are linearized in the vicinity of the steady-state error $\tilde{\vartheta}_{\mathrm{m}0}$, yielding

$$\frac{\mathrm{d}}{\mathrm{d}t}\begin{bmatrix}\tilde{\psi}_{\mathrm{d}}\\\tilde{\psi}_{\mathrm{q}}\end{bmatrix}=\begin{bmatrix}k_1 & -k_1\frac{\beta_{\mathrm{num}}}{\beta_{\mathrm{den}}}+\omega_{\mathrm{m}}\\k_2-\omega_{\mathrm{m}} & -k_2\frac{\beta_{\mathrm{num}}}{\beta_{\mathrm{den}}}\end{bmatrix}\begin{bmatrix}\tilde{\psi}_{\mathrm{d}}\\\tilde{\psi}_{\mathrm{q}}\end{bmatrix}.\tag{18}$$

The stability of the reduced-order observer is studied in no-load condition and with the rated load, with actual parameters $L_{\mathrm{d}}=2.00$ p.u., $L_{\mathrm{q}}=0.33$ p.u., and $R_{\mathrm{s}}=0.04$ p.u. of the 6.7-kW SyRM. The same relative uncertainty is assumed for all three model parameters $\hat{L}_{\mathrm{d}}$, $\hat{L}_{\mathrm{q}}$, and $\hat{R}_{\mathrm{s}}$. Hence, eight different worst-case combinations, consisting of minimum and maximum values of the model parameters, can be formed. For example, if the relative uncertainty is defined to be 20%, one of the worst-case combinations is $\hat{L}_{\mathrm{d}}=0.8L_{\mathrm{d}}$, $\hat{L}_{\mathrm{q}}=1.2L_{\mathrm{q}}$, and $\hat{R}_{\mathrm{s}}=0.8R_{\mathrm{s}}$.

At each studied operating point, the local stability of the system was analyzed for all eight worst-case combinations of erroneous model parameters. First, the estimation error of the rotor position (14) was analytically solved in steady state. Then, the stability of the linearized system (18) was checked.

The stability of the estimation-error dynamics with erroneous model parameters was analyzed for different values of the design parameters $b$ and $c$. The stability maps for the reduced-order observer are depicted in Fig. 1. Fig. 1(a) shows an example of the stability map in the design-parameter space for the parameter uncertainties of 10%, 20%, and 30%. The vertical axis is scaled with the inverse rotor speed in order to

help the comparison at different speeds. The operating point is defined by $\omega_{\mathrm{m}}=0.1$ p.u., $i_{\mathrm{d}}=0.5$ p.u., and $i_{\mathrm{q}}=0$. In Fig. 1(b), the stability maps for the parameter uncertainties of 20% are depicted for three different values of $i_{\mathrm{q}}$. The values for $i_{\mathrm{q}}$ are $-0.8$ p.u., 0, and 0.8 p.u. It can be seen that the shape of the stable area remains approximately unchanged when the load is varied.

### C. Adaptive Full-Order Observer

The estimation error dynamics of the adaptive full-order observer are linearized in the vicinity of the steady-state error $\tilde{\vartheta}_{\mathrm{m}0}$, yielding (19) shown at the top of the page. With accurate model parameters, $\hat{\beta}\beta_{\mathrm{den}}-\beta_{\mathrm{num}}=0$, and the characteristic polynomial of (19) can be written as (12).

The stability of the full-order observer is studied in no-load condition and with the rated load. At each studied operating point, the local stability of the system was analyzed for all eight worst-case combinations of erroneous model parameters. First, the estimation errors of the rotor position (14) and the flux components (16) were analytically solved in the steady state. Then, the stability of the linearized system (19) was checked.

The stability of the estimation-error dynamics with erroneous model parameters was analyzed for different values of the design parameters $b$, $c$, and $\rho$. Fig. 2(a) shows an example of the stability map in the design-parameter space for the parameter uncertainties of 10%, 20%, and 30% in a fashion similar to Fig. 1(a). The operating point in Fig. 2(a) is defined by $\omega_{\mathrm{m}}=0.1$ p.u., $i_{\mathrm{d}}=0.5$ p.u., $i_{\mathrm{q}}=0$, and $\rho=2$ p.u. It can be seen that the region of $b$ and $c$ yielding the stable operation is large even in the case of the parameter uncertainty of 20%. As the parameter uncertainty increases, the stable region shrinks (and disappears if the uncertainty is high enough).

In Figs. 2(b)–2(d), the stability maps for the parameter uncertainties of 20% are depicted for three different values of $\omega_{\mathrm{m}}$, $\rho$, and $i_{\mathrm{q}}$, respectively. The values for $\omega_{\mathrm{m}}$ in Fig. 2(b) are 0.1 p.u., 0.3 p.u., and 0.50 p.u. The values for $\rho$ in Fig. 2(c) are 1 p.u., 2 p.u., and 3 p.u. The values for $i_{\mathrm{q}}$ in Fig. 2(d) are $-0.8$ p.u., 0, and 0.8 p.u. It can be seen that the area of stable operation is virtually insensitive to changes in the parameter $\rho$. The size of the stable region depends on the speed and the current components, but its shape remains approximately unchanged.

## V. EXPERIMENTAL SETUP AND PARAMETERS

The motion-sensorless control system was implemented on a dSPACE DS1104 PPC/DSP board. A 6.7-kW four-pole SyRM was fed by a frequency converter that is controlled by
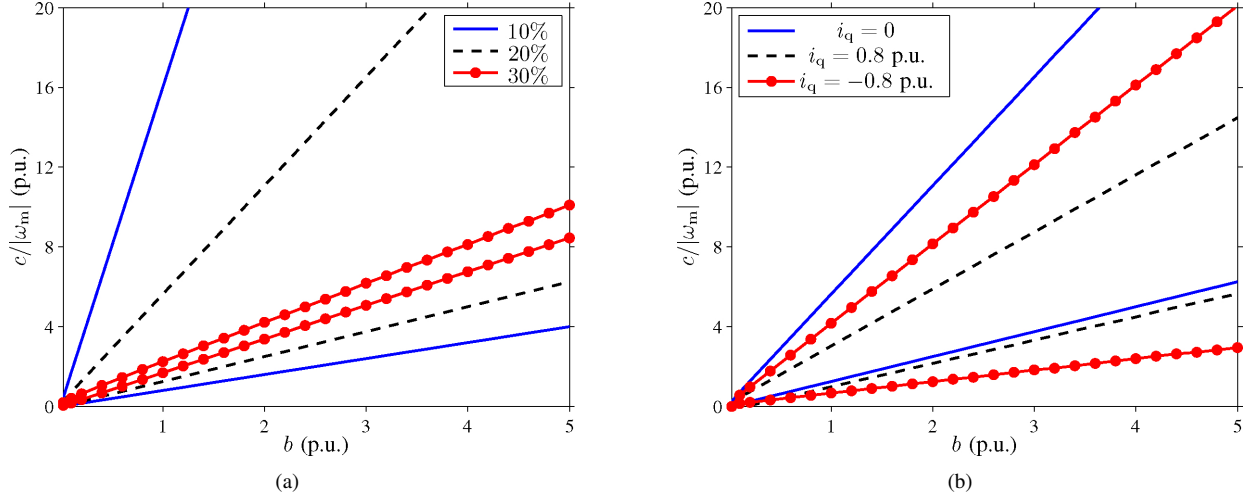
Fig. 1. Stability maps in the design-parameter space for the reduced-order observer: (a) areas of stable operation for 10%, 20% and 30% parameter uncertainties, and (b) areas of stable operation for $i_q = 0$, $i_q = 0.8$ p.u. and $i_q = -0.8$ p.u. with 20% parameter uncertainties. The d-axis current $i_d = 0.5$ p.u. and $\omega_m = 0.1$ p.u.

the DS1104 board. The rated values of the SyRM are: speed 3175 r/min; frequency 105.8 Hz; line-to-line rms voltage 370 V; rms current 15.5 A; and torque 20.1 Nm. The base values for angular speed, voltage, and current are defined as $2\pi \cdot 105.8$ rad/s, $\sqrt{2/3} \cdot 370$ V, and $\sqrt{2} \cdot 15.5$ A, respectively. A servo motor was used as a loading machine. The rotor speed $\omega_m$ and position $\vartheta_m$ were measured using an incremental encoder for monitoring purposes.

The stator currents and the dc-link voltage were measured, and the reference voltage obtained from the current controller was used for the observer. The sampling was synchronized to the modulation, and both the switching frequency and the sampling frequency were 8 kHz. A simple current feedforward compensation for dead times and power device voltage drops was applied.

The control system was augmented with a speed controller, whose feedback signal was the speed estimate $\hat{\omega}_m$ obtained from the proposed observer. The bandwidth of this PI control loop, including active damping, was $2\pi \cdot 5.3$ rad/s (0.05 p.u.). The estimate of the per-unit electromagnetic torque was evaluated as

$$\hat{T}_e = (\hat{L}_d - \hat{L}_q)i_d i_q. \tag{20}$$

The gain values were chosen based on empirical results. The gain $b = 2$ p.u. was used for the reduced-order observer in (5). For the adaptive full-order observer, the gains were: $c = 2b|\hat{\omega}_m|$, $\rho = 2$ p.u., and

$$b = \begin{cases} |\hat{\omega}_m|, & \text{if } \hat{\omega}_m \geq 0.05 \text{ p.u.} \\ 0.05 \text{ p.u.}, & \text{otherwise.} \end{cases} \tag{21}$$

The effects of the magnetic saturation on the inductances

### TABLE I
### Per-Unit Parameters for Saturation Model

| $L_{du}$ | $L_{qu}$ | $\alpha$ | $\gamma$ | $\delta$ | $i_\Delta$ |
|---|---|---|---|---|---|
| 3.15 | 0.685 | 2.24 | 0.353 | 0.085 | 0.2 |

have been modeled as functions of the measured current [15]

$$\hat{L}_d = \begin{cases} L_{du} - \alpha i_d - \delta \left| \frac{i_q}{i_\Delta} \right|, & \text{if } i_d \leq i_\Delta \\ L_{du} - \alpha i_d - \delta \left| \frac{i_q}{i_d} \right|, & \text{otherwise} \end{cases} \tag{22a}$$

$$\hat{L}_q = \begin{cases} L_{qu} - \gamma\sqrt{|i_q|} - \delta \left| \frac{i_d}{i_\Delta} \right|, & \text{if } i_q \leq i_\Delta \\ L_{qu} - \gamma\sqrt{|i_q|} - \delta \left| \frac{i_d}{i_q} \right|, & \text{otherwise} \end{cases} \tag{22b}$$

where $i_\Delta$ is a transition value to avoid divisions by small numbers. The saturation model parameters are given in Table I. The model stator resistance is $\hat{R}_s = 0.042$ p.u.

## VI. Experimental Results

Fig. 3 shows the effect of the parameter errors on the position estimation error at the speed of 0.1 p.u. with 50% rated load torque applied. The reduced-order observer is used in Fig. 3(a), and the adaptive full-order observer is used in Fig. 3(b). The measured data is captured by varying each model parameter from 90% up to 110% of the actual value in 10 seconds. The predicted error is obtained utilizing (14), (20), and (22). The predicted errors are in good agreement with the measured error.

It can be seen that the model parameters $\hat{R}_s$ and $\hat{L}_q$ have only a moderate effect on the position error, whereas the incorrect value of $\hat{L}_d$ evidently increases the estimation error in Fig. 3(a), when the reduced-order observer is used. According to Fig. 3(b), the adaptive full-order observer is less sensitive to parameter errors. This is due to the smaller values of the design parameters $b$ and $c$ used for the adaptive full-order observer, which reduces the sensitivity to parameter errors as stated in Section IV. It should be noted that the
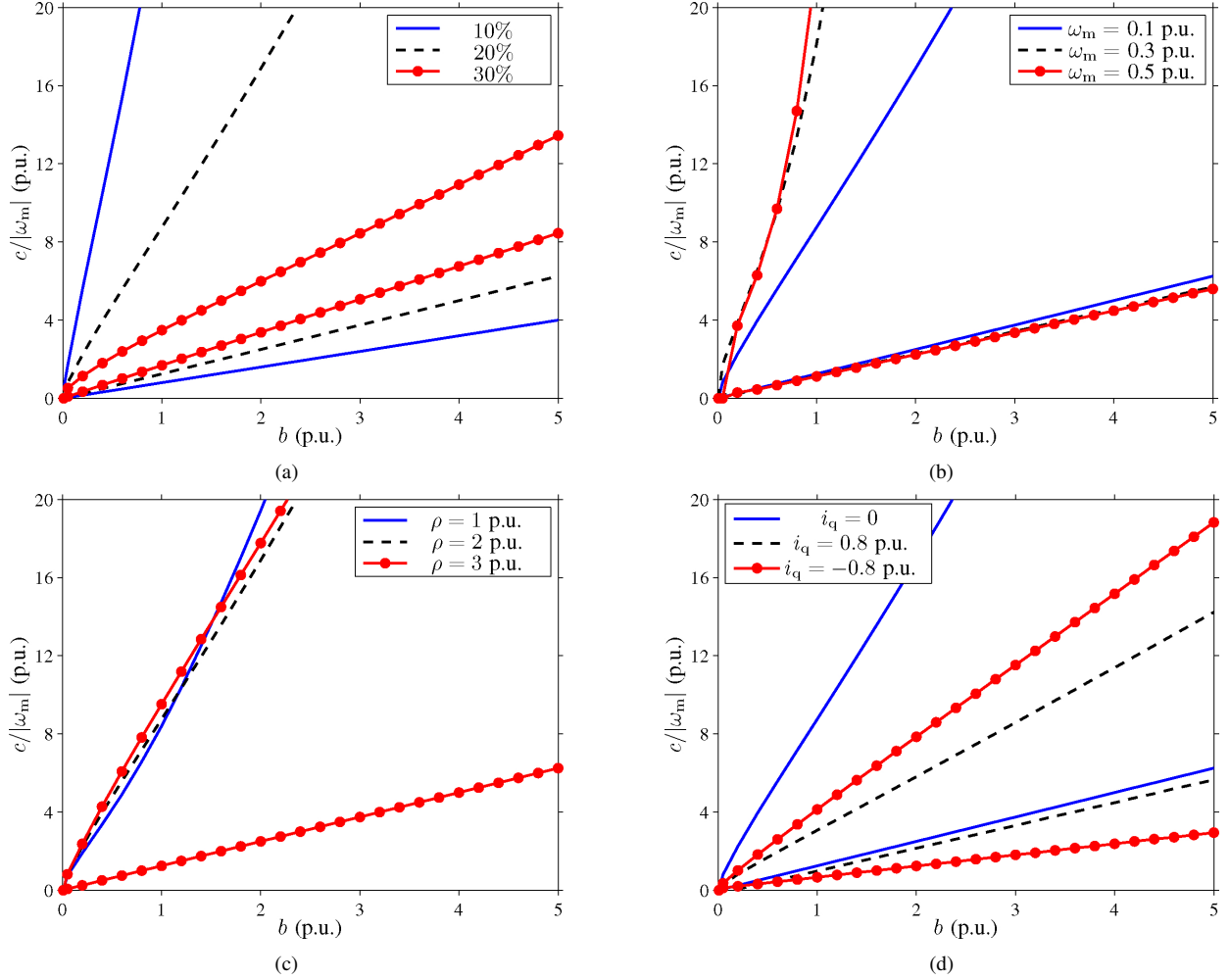
Fig. 2. Stability maps in the design-parameter space for the adaptive full-order observer: (a) areas of stable operation for 10%, 20% and 30% parameter uncertainties, (b) areas of stable operation for $\omega_{\mathrm{m}} = 0.1$ p.u., $\omega_{\mathrm{m}} = 0.3$ p.u. and $\omega_{\mathrm{m}} = 0.5$ p.u. with 20% parameter uncertainties, (c) areas of stable operation for $\rho = 1$ p.u., $\rho = 2$ p.u. and $\rho = 3$ p.u. with 20% parameter uncertainties, and (d) areas of stable operation for $i_{\mathrm{q}} = 0$, $i_{\mathrm{q}} = 0.8$ p.u. and $i_{\mathrm{q}} = -0.8$ p.u. with 20% parameter uncertainties. The d-axis current is $i_{\mathrm{d}} = 0.5$ p.u., $\omega_{\mathrm{m}} = 0.1$ p.u. in (a,c,d), and $\rho = 2$ p.u. in (a,b,d).

relative errors of $\hat{L}_{\mathrm{d}}$ and $\hat{L}_{\mathrm{q}}$ are defined with respect to the (original) operating point values. As the estimation error increases, the actual values of $i_{\mathrm{d}}$ and $i_{\mathrm{q}}$ change, resulting in changes in the actual values of $L_{\mathrm{d}}$ and $L_{\mathrm{q}}$ due to the magnetic saturation.

Experimental results of a stepwise speed reversal from 0.1 p.u. to $-0.1$ p.u. and back to 0.1 p.u. with the rated load torque applied are depicted in Fig. 4. The reduced-order observer is used in Fig. 4(a), and the adaptive full-order observer is used in Fig. 4(b). It can be seen that the reduced-order observer amplifies the estimation noise in the regenerating mode in Fig. 4(a). This behavior is analyzed in [15]. With the adaptive full-order observer, the amplitude of the estimation noise does not depend on the operating mode, as seen in Fig. 4(b).

When the reduced-order observer is used, saturation-induced harmonics cause noise in the position estimate in the regenerating mode if the machine is highly saturated [15]. Results of a slow change of $i_{\mathrm{d}}$ from 0.3 p.u. to 0.5 p.u. at the speed 0.1 p.u. with $-50\%$ rated load torque applied are shown in Fig. 5. The reduced-order observer is used in Fig. 5(a), and the adaptive full-order observer is used in Fig. 5(b). It can

be seen that as $i_{\mathrm{d}}$ increases in the regenerating mode, the noise in the position estimate of the reduced-order observer increases, but the adaptive full-order observer is not sensitive to the harmonics.

Experimental results of load-torque steps when the speed reference was kept at 0.05 p.u. are shown in Fig. 6. The load torque was stepped to $-75\%$ of the rated load torque at $t = 2.5$ s, reversed at $t = 7.5$ s, and removed at $t = 12.5$ s. The reduced-order observer is used in Fig. 6(a), and the adaptive full-order observer is used in Fig. 6(b). It can be seen that the observers behave well in load transients in low-speed operation.

## VII. CONCLUSIONS

In this paper, a reduced-order observer and an adaptive full-order observer were compared for motion-sensorless synchronous motor drives. Furthermore, a stabilizing gain was proposed for the full-order observer; the proposed gain guarantees the local stability of the closed-loop system, if the motor parameters are known. Equations for the steady-state position error and for the linearized estimation-error dynamics under
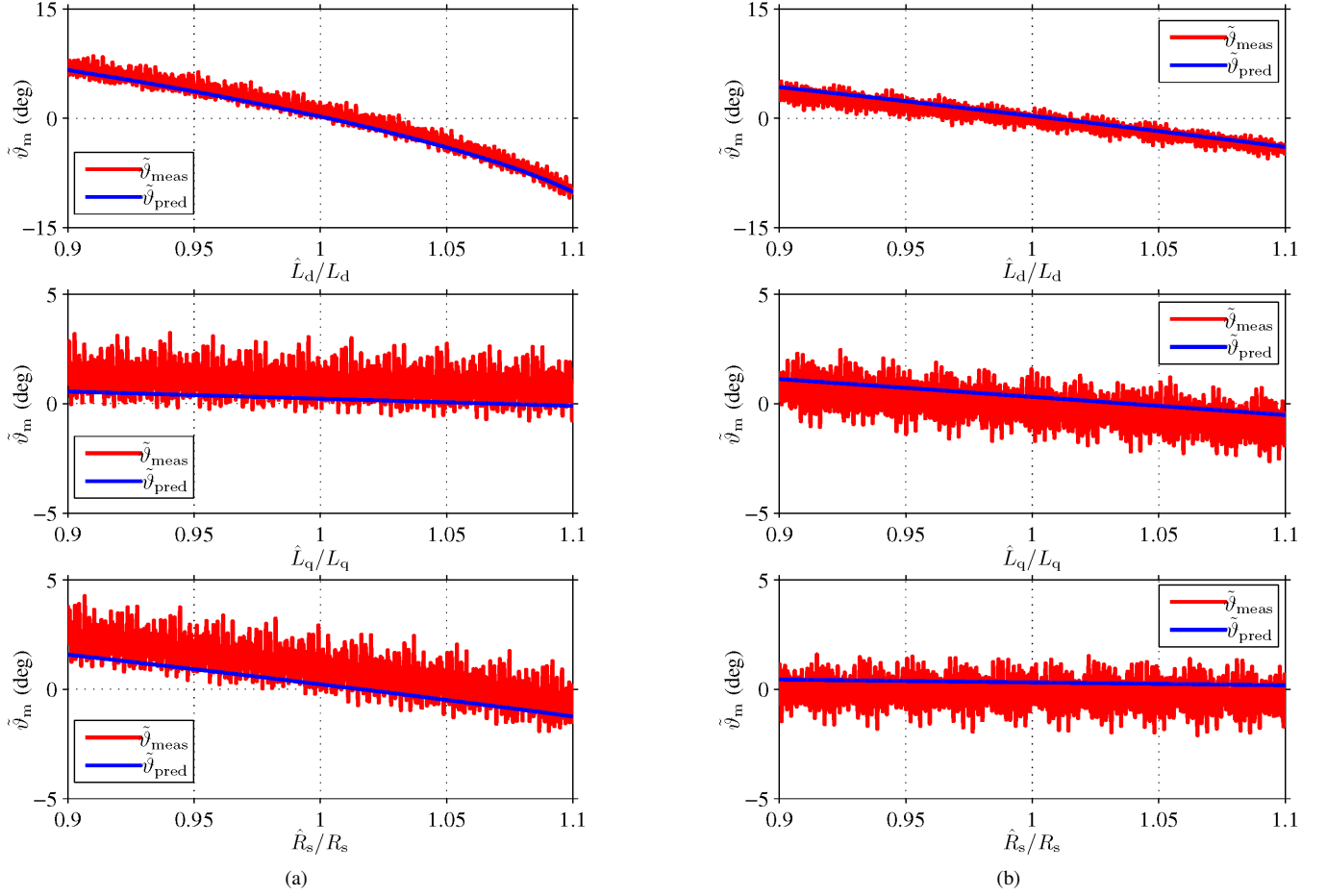
Fig. 3.  Measured errors and predicted errors in the position estimate at 0.1-p.u. speed with 50% rated load torque applied: (a) reduced-order observer and (b) adaptive full-order observer. The d-axis current is 0.4 p.u. The measured data is captured by varying each model parameter from 90% up to 110% of the actual value in 10 seconds.
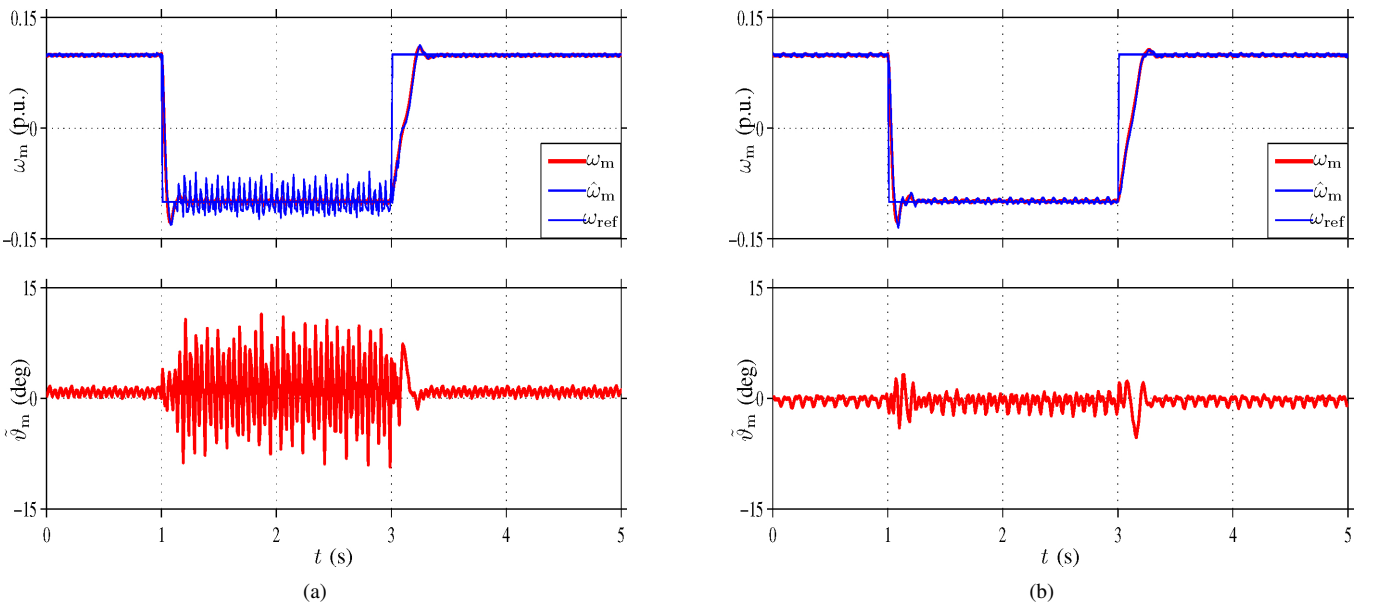


Fig. 4.  Experimental results of a stepwise speed reversal (0.1 p.u. $\rightarrow$ $-0.1$ p.u. $\rightarrow$ 0.1 p.u.) with rated load torque applied: (a) reduced-order observer, (b) adaptive full-order observer. The d-axis current is 0.5 p.u.
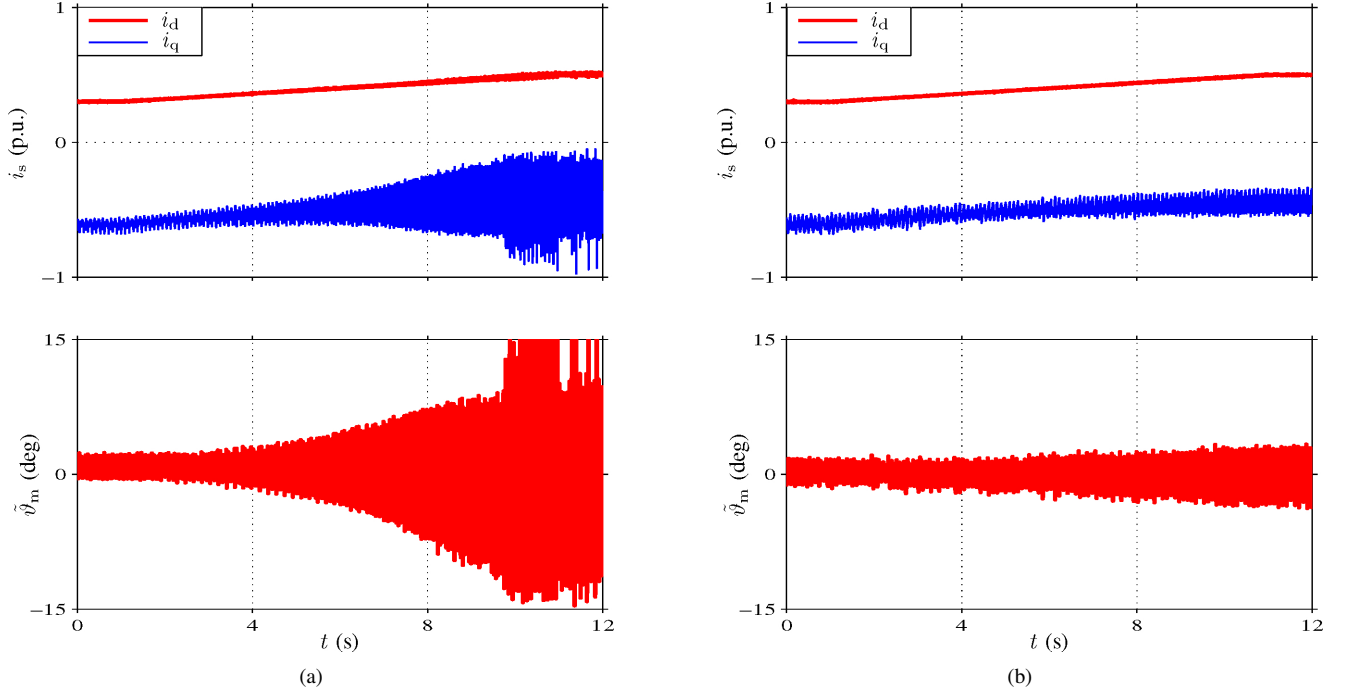
Fig. 5. Experimental results of a slow change in $i_{\mathrm{d}}$ from 0.3 p.u. to 0.5 p.u. with $-50\%$ rated load torque applied: (a) reduced-order observer, (b) adaptive full-order observer.
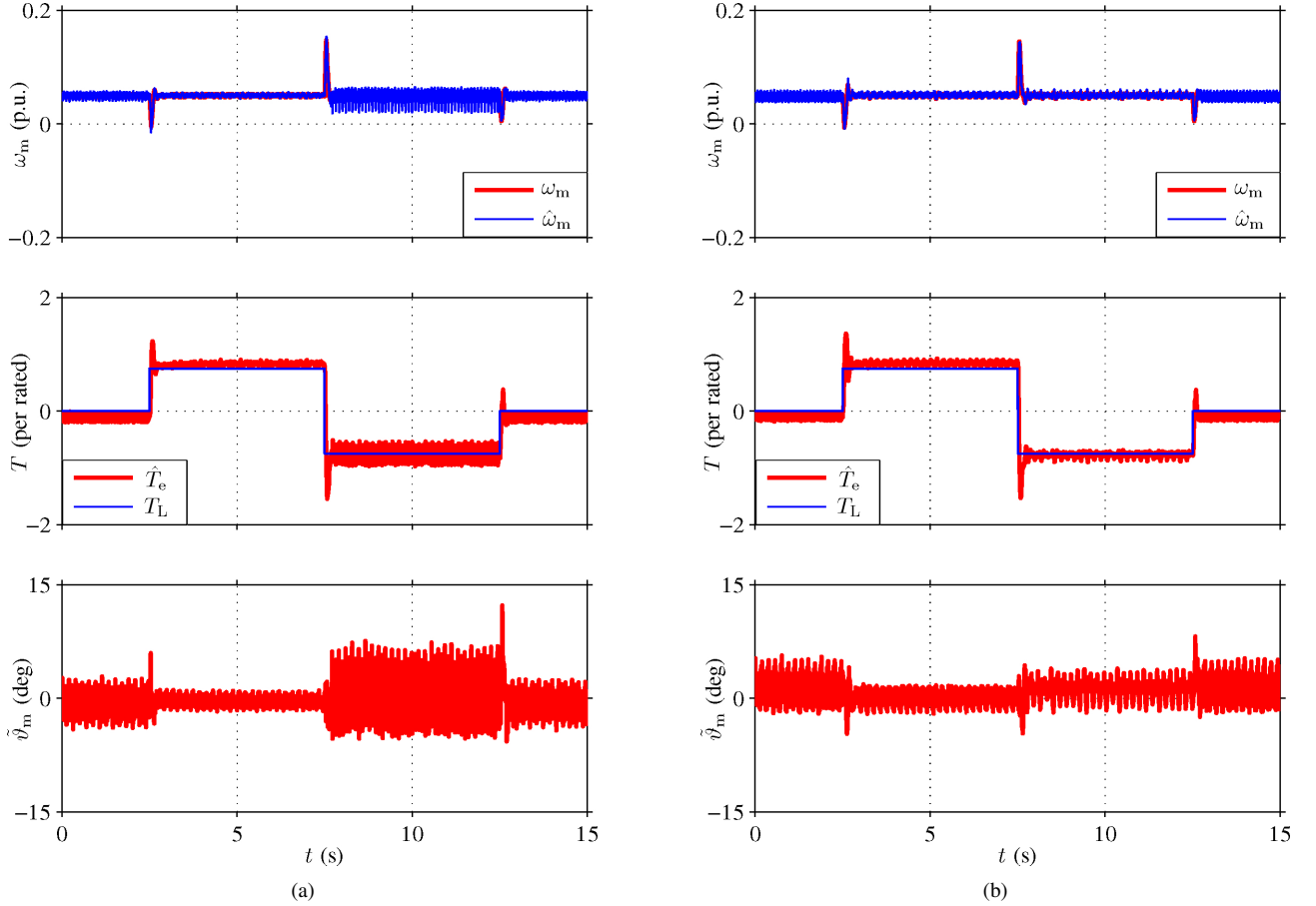


Fig. 6. Experimental results showing load-torque steps ($0 \rightarrow -75\%$ rated $\rightarrow 75\%$ rated) when the speed reference is kept at 0.05 p.u.: (a) reduced-order observer, (b) adaptive full-order observer. $T_{\mathrm{L}}$ shown in the second subplot is the torque reference of the loading drive. The d-axis current is 0.4 p.u.

erroneous model parameters were derived, and the robustness of the two observers against parameter errors was analyzed and compared. The reduced-order observer is simpler and easier to tune than the full-order observer, and it could easily be augmented with stator-resistance adaptation. On the other hand, analytical and experimental results indicate that the full-order observer can be made less sensitive to model parameter uncertainties and noise—without sacrificing its dynamic performance—than the reduced-order observer.

## REFERENCES

[1] R. Lagerquist, I. Boldea, and J. Miller, "Sensorless control of the synchronous reluctance motor," *IEEE Trans. Ind. Appl.*, vol. 30, no. 3, pp. 673–682, May/June 1994.

[2] E. Capecchi, P. Guglielmo, M. Pastorelli, and A. Vagati, "Position-sensorless control of the transverse-laminated synchronous reluctance motor," *IEEE Trans. Ind. Appl.*, vol. 37, no. 6, pp. 1768–1776, Nov./Dec. 2001.

[3] H. F. Hofmann, S. R. Sanders, and A. EL-Antably, "Stator-flux-oriented vector control of synchronous reluctance machines with maximized efficiency," *IEEE Trans. Ind. Electron.*, vol. 51, no. 5, pp. 1066–1072, Oct. 2004.

[4] J.-I. Ha, S.-J. Kang, and S.-K. Sul, "Position-controlled synchronous reluctance motor without rotational transducer," *IEEE Trans. Ind. Appl.*, vol. 35, no. 6, pp. 1393–1398, Nov./Dec. 1999.

[5] A. Consoli, G. Scarcella, G. Scelba, A. Testa, and D. A. Triolo, "Sensorless rotor position estimation in synchronous reluctance motors exploiting a flux deviation approach," *IEEE Trans. Ind. Appl.*, vol. 43, no. 5, pp. 1266–1273, Sep./Oct. 2007.

[6] R. Morales-Caporal and M. Pacas, "Encoderless predictive direct torque control for synchronous reluctance machines at very low and zero speed," *IEEE Trans. Ind. Electron.*, vol. 55, no. 12, pp. 4408–4416, Dec. 2008.

[7] M. J. Corley and R. D. Lorenz, "Rotor position and velocity estimation for a salient-pole permanent magnet synchronous machine at standstill and high speeds," *IEEE Trans. Ind. Appl.*, vol. 34, no. 4, pp. 784–789, Jul./Aug. 1998.

[8] A. Piippo, M. Hinkkanen, and J. Luomi, "Sensorless control of PMSM drives using a combination of voltage model and HF signal injection," in *Conf. Rec. IEEE-IAS Annu. Meeting*, vol. 2, Seattle, WA, Oct. 2004, pp. 964–970.

[9] O. Wallmark, L. Harnefors, and O. Carlson, "An improved speed and position estimator for salient permanent-magnet synchronous motors," *IEEE Trans. Ind. Electron.*, vol. 52, no. 1, pp. 255–262, Feb. 2005.

[10] W. Hammel and R. M. Kennel, "Position sensorless control of PMSM by synchronous injection and demodulation of alternating carrier voltage," in *Proc. IEEE SLED 2010*, Padova, Italy, July 2010, pp. 56–63.

[11] A. Piippo, M. Hinkkanen, and J. Luomi, "Analysis of an adaptive observer for sensorless control of interior permanent magnet synchronous motors," *IEEE Trans. Ind. Electron.*, vol. 55, no. 2, pp. 570–576, Feb. 2008.

[12] M. Hinkkanen, T. Tuovinen, L. Harnefors, and J. Luomi, "A combined position and stator-resistance observer for salient PMSM drives: design and stability analysis," *IEEE Trans. Power Electron.*, vol. 27, no. 2, pp. 601–609, Feb. 2012.

[13] S. Sangwongwanich, S. Suwankawin, S. Po-ngam, and S. Koonlaboon, "A unified speed estimation design framework for sensorless ac motor drives based on positive-real property," in *Proc. PCC-Nagoya'07*, Nagoya, Japan, Apr. 2007, pp. 1111–1118.

[14] A. Piippo and J. Luomi, "Torque ripple reduction in sensorless PMSM drives," in *Proc. IEEE IECON'06*, Paris, France, Nov. 2006, pp. 920–925.

[15] T. Tuovinen, M. Hinkkanen, and J. Luomi, "Analysis and design of a position observer with resistance adaptation for synchronous reluctance motor drives," in *Proc. IEEE ECCE'11*, vol. 1, Phoenix, AZ, Sep. 2011, pp. 88–95.

[16] G. Yang, R. Tomioka, M. Nakano, and T. H. Chin, "Position and speed sensorless control of brushless DC motor based on an adaptive observer," *IEEJ Trans. Ind. Appl.*, vol. 113, pp. 579–586, May 1993.

[17] L. Harnefors and H.-P. Nee, "A general algorithm for speed and position estimation of AC motors," *IEEE Trans. Ind. Electron.*, vol. 47, no. 1, pp. 77–83, Feb. 2000.

**Toni Tuovinen** received the M.Sc. degree from the University of Helsinki, Helsinki, Finland, in 2005, and the M.Sc.(Eng.) degree from Helsinki University of Technology, Espoo, Finland, in 2009.

Since 2007, he has been with the Helsinki University of Technology (part of Aalto University since 2010). He is currently a Research Scientist in the Aalto University School of Electrical Engineering, Espoo, Finland. His main research interest is the control of electric drives.

**Marko Hinkkanen** (M'06) received the M.Sc.(Eng.) and D.Sc.(Tech.) degrees from the Helsinki University of Technology, Espoo, Finland, in 2000 and 2004, respectively.

Since 2000, he has been with the Helsinki University of Technology (part of Aalto University since 2010). He is currently an Adjunct Professor in the Aalto University School of Electrical Engineering, Espoo, Finland. His research interests include electric drives and electric machines.

**Lennart Harnefors** (S'93–M'97–SM'08) was born in 1968 in Eskilstuna, Sweden. He received the M.Sc., Licentiate, and Ph.D. degrees in electrical engineering from the Royal Institute of Technology, Stockholm, Sweden, and the Docent (D.Sc.) degree in industrial automation from Lund University, Lund, Sweden, in 1993, 1995, 1997, and 2000, respectively.

From 1994 to 2005, he was with Mälardalen University, Västerås, Sweden, where he, in 2001, was appointed as a Professor of electrical engineering. From 2001 to 2006, he was also a part-time Visiting Professor of electrical drives with Chalmers University of Technology, Göteborg, Sweden. He is currently an R&D Project Manager with ABB, Power Systems - HVDC, Ludvika, Sweden and an Adjunct Professor of power electronics with the Royal Institute of Technology, Stockholm, Sweden. His research interests include grid-connected converters and ac drives.

Dr. Harnefors is an Associate Editor of the IEEE TRANSACTIONS ON INDUSTRIAL ELECTRONICS and the *International Journal of Power Electronics*. He was the recipient of the 2000 ABB Gunnar Engström Energy Award and the 2002 IEEE TRANSACTIONS ON INDUSTRIAL ELECTRONICS Best Paper Award.

**Jorma Luomi** (M'92) received the M.Sc.(Eng.) and D.Sc.(Tech.) degrees from the Helsinki University of Technology, Espoo, Finland, in 1977 and 1984, respectively.

He joined the Helsinki University of Technology in 1980, and from 1991 to 1998, he was a Professor at Chalmers University of Technology, Göteborg, Sweden. Since 1998, he was a Professor in the Helsinki University of Technology (part of Aalto University since 2010), Espoo, Finland. His research interests included electric drives, electric machines, and numerical analysis of electromagnetic fields.

Prof. Luomi passed away in December 2011.